2-1-2000

Quantum Calculations On The Vibrational Predissociation Of NeBr2: Evidence For Continuum Resonances

Thomas Alex Stephenson
Swarthmore College, tstephe1@swarthmore.edu

N. Halberstadt

Quantum calculations on the vibrational predissociation of NeBr 2 : Evidence for continuum resonances

Thomas A. Stephenson and Nadine Halberstadt

Citation: The Journal of Chemical Physics **112**, 2265 (2000); doi: 10.1063/1.480791
View online: http://dx.doi.org/10.1063/1.480791
View Table of Contents: http://scitation.aip.org/content/aip/journal/jcp/112/5?ver=pdfcov
Published by the AIP Publishing

Quantum calculations on the vibrational predissociation of $NeBr_2$: Evidence for continuum resonances

Thomas A. Stephenson
Department of Chemistry, Swarthmore College, Swarthmore, Pennsylvania 19081

Nadine Halberstadt
LPQT-IRSAMC, Université Paul Sabatier et CNRS, 31062 Toulouse Cedex, France

(Received 3 August 1999; accepted 1 November 1999)

Quantum mechanical calculations on the vibrational predissociation dynamics of $NeBr_2$ in the B electronic state have been performed and the results compared with both experimental data and other computational studies. For vibrational levels with $v \leqslant 20$ we find that the vibrational state dependence of the predissociation lifetimes is in qualitative agreement with experimental measurements, as are the calculated Br_2 fragment rotational distributions. For higher vibrational levels, the $B \leftarrow X$ excitation profiles are well represented by a sum of two Lorentzian line shapes. We attribute this result to the presence of long-lived resonances in the dissociative continuum that are reminiscent of long-lived dissociative trajectories in previous classical studies of $NeBr_2$. © *2000 American Institute of Physics.* [S0021-9606(00)00205-1]

I. INTRODUCTION

One of the most useful tools applied to understand the dynamics on multidimensional potential energy surfaces has been accurate three-dimensional quantum mechanical calculations.[1] Of particular note have been the insights obtained from a detailed theoretical analysis of the dynamics of the van der Waals complexes composed of a rare gas atom and a diatomic halogen molecule.[2–25] These studies have reproduced a large quantity of experimentally determined parameters, such as binding energies, vibrational predissociation lifetimes, and fragment vibrational and rotational distributions. In some cases, the confidence assigned to the calculated quantities is sufficient to allow tests of model rare gas/halogen potential energy surfaces.[18,19,24] In other situations, the calculations have provided physical models for the dissociation of complexes, such as the demonstration of intramolecular vibrational redistribution in the dissociation of the $ArCl_2$ complex.[4,24]

At the same time, others have sought to use classical or semiclassical methods to understand features of the dissociation in the context of more conceptually transparent models. These efforts have met with mixed success. Waterland *et al.*, developed a semiclassical model that reproduced many of the features of the ICl rotational distributions produced following fragmentation of HeICl.[26] This approach was also applied by Stephenson to the IBr fragment distributions that result from the dissociation of NeIBr (Ref. 27) and by Nejad-Sattari and Stephenson to the dissociation of $NeBr_2$.[28] For these species, the agreement of the semiclassical model ranged from excellent (NeIBr dissociation[27]) to fair ($NeBr_2$).[28] (Nejad-Sattari and Stephenson explored the origin of this lack of consistent performance in a previous publication.[28]) Common to both of these latter studies has been the appearance, at low values of the total energy available for fragment internal and translational excitation (E_{avl}), of long-lived ''orbiting resonance'' features in the classical dynamics. The possibility that these classical structures might have a counterpart in the quantum dynamics of $NeBr_2$ forms a principle motivation for this work; we summarize the classical results in more detail in Sec. II.

The quantum dynamics of rare gas/halogen complexes with low values of fragment energy have been examined previously. González-Lezana *et al.* investigated the excitation cross sections and fragment rotational distributions for a number of $HeBr_2$ vibrational levels.[22] They note the presence of very complicated structures in the energy dependent dissociation cross sections, and suggest that long-lived resonances in the dissociation continuum may be the cause. In a separate examination of the low energy dynamics of $ArCl_2$, Janda *et al.* demonstrate that long-lived resonances are present in the continuum at low values of E_{avl}, and suggest that these might be thought of as rotationally predissociative states.[24] The impact of the resonances is strongly dependent on the parameters used in the model intermolecular potential, with modest fine-tuning of the potential producing significant oscillation in the fragment rotational distributions and order of magnitude changes in the calculated dissociation lifetimes.

The $NeBr_2$ van der Waals molecule has been the subject of considerable experimental investigation. This species was first observed by Swartz *et al.* using laser-induced fluorescence excitation spectroscopy.[29] The excitation feature corresponding to vibrational levels $v = 11-30$ in the B electronic state were observed with modest resolution. In higher resolution experiments, Janda and coworkers resolved the rotational structure associated with several $B \leftarrow X$ transitions in $NeBr_2$ and demonstrated conclusively that the molecule assumes a T-shaped equilibrium structure.[30,31] Predissociation lifetimes were determined from an analysis of the homogeneous linewidths of the features observed. Most recently, Nejad-Sattari and Stephenson have reported on the Br_2 fragment rotational distributions that result from the dis-

sociation of $NeBr_2$.[28] This work considered dissociation channels resulting in the loss of one and two quanta of Br_2 vibrational excitation. Energetic constraints were found to limit the disposal of energy into the fragment rotational degree of freedom, as the distributions uniformly extended to the highest rotational level that is energetically possible. The abrupt termination of certain rotational distributions was used to refine the dissociation energy of $NeBr_2$; D_0 for the X state, $v=0$ was found to be 70.0 ± 1.1 cm^{-1}.[28]

In this manuscript, we report on our quantum calculations on the dynamics of the $NeBr_2$ molecule in the B electronic state. In Sec. II, we briefly summarize the previous classical trajectory calculations that motivated this work, followed by a concise description of our computational methodology. In Secs. IV and V, we present the results of the calculations, and discuss the implications of this work in light of the abundant experimental and computational data on the dynamics of rare gas/halogen systems.

II. SUMMARY OF CLASSICAL CALCULATIONS

In the approach developed by Waterland *et al.*,[26] and applied to $NeBr_2$ by Nejad-Sattari and Stephenson,[28] a rare gas/halogen van der Waals complex is assumed prepared in a quasibound state correlating with vibrational state v of an excited electronic state by laser excitation. The complex is then transferred to the repulsive wall of the van der Waals potential correlating with fragment vibrational level $v-1$. This transfer is assumed to occur instantaneously and without any consideration of the dynamics of the intramolecular vibrational coupling mechanism. The fragment rotational distribution then arises from the scattering of the rare gas atom from the repulsive wall of the van der Waals potential. The energy available to the fragments (E_{avl}) is then the diatomic vibrational spacing, less the dissociation energy of the complex. Exact classical trajectories propagated on the potential energy surface provide a unique value for the fragment rotational angular momentum for each initial condition. The initial conditions are sampled in accord with the known energetics of the dissociation and the amplitude of the rare gas/halogen quasibound wave function. Complete details of this method can be found in Refs. 27 and 28.

This model, when applied to the IBr fragments that result from the dissociation of NeIBr, provided an excellent fit to the experimental fragment rotational distribution.[27] When the semiclassical model was applied, however, to the $NeBr_2$ complex, the agreement with the experimental Br_2 fragment rotational distributions was much less satisfying.[28] One of the intriguing results of the classical trajectory calculations on both NeIBr and $NeBr_2$ was the observation of ''orbiting resonance'' structures at relatively low values of fragment energy.[27,28] Specifically, complexes dissociating near the threshold for loss of only one quantum of Br_2 (or IBr) vibrational excitation have small values of E_{avl}. Under these circumstances, recoil of the fragments is far from prompt, with multiple encounters occurring with the repulsive wall of the rare gas/halogen intermolecular potential. The analysis of this phenomenon provided by Nejad-Sattari and Stephenson for $NeBr_2$ demonstrates that these resonances occur when the recoiling rare gas atom samples a region of high angular anisotropy in the intermolecular potential energy surface.[28] Since in Hamilton's equations of motion the angular anisotropy of the potential energy is associated with the time rate of change of the angular momentum, the result is excitation of the Br_2 rotational motion, counterbalanced by the orbital angular momentum of the Ne atom such that the total angular momentum is conserved. At high and moderate values of E_{avl}, this effect is simply the classical origin of the calculated fragment rotational excitation. At low E_{avl}, however, the degree of excitation of the diatomic fragment rotational angular momentum at short times in the trajectory is larger than that consistent with the total fragment energy at infinite separation. In other words, conservation of energy traps the fragments in the attractive portion of the intermolecular potential until a second collision with the repulsive wall serves to quench some of the fragment angular momentum. In Fig. 1, we display a sample trajectory from these previous calculations, along with a plot of the Br_2 fragment rotational angular momentum as a function of time. The goal of the present calculations is to explore, using the same potential energy surface as employed in the classical calculations, the presence or absence of signatures in the quantum dynamics that resemble the classical ''orbiting resonances'' observed in the previous investigations.

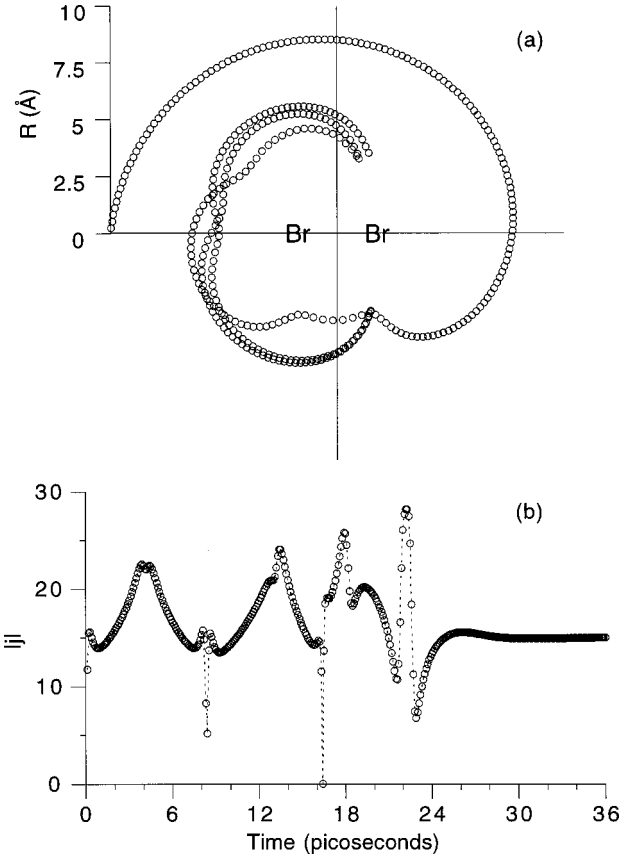

FIG. 1. Classical trajectory results on $NeBr_2$, with $E_{avl}=12.9\,cm^{-1}$. Total integration time=36 ps, with a step size of 0.1 ps. (a) Position of the Ne atom relative to the Br–Br internuclear axis. (b) Br_2 angular momentum (in units of $\hbar$) as a function of time.

III. QUANTUM METHODOLOGY

The calculations presented in this manuscript follow the methodology described in detail by Halberstadt *et al.*[4] Briefly, we write the Hamiltonian operator for $NeBr_2$ as,

$$-\frac{\hbar^2}{2m}\frac{\partial^2}{\partial R^2}-\frac{\hbar^2}{2\mu}\frac{\partial^2}{\partial r^2}+\frac{l^2}{2mR^2}+\frac{j^2}{2\mu r^2}+V_{Br_2}(r)+W(r,R,\theta), \tag{1}$$

where r is the magnitude of the vector between the Br atoms, R is the magnitude of the vector between the Ne atom and the center of mass of Br_2, and θ is the angle between these two vectors. The function $W(r,R,\theta)$ is the ''intermolecular'' potential energy for the motion of the Ne atom relative to the center-of-mass of Br_2. The corresponding reduced mass is m. The Br–Br potential energy function is $V_{Br_2}(r)$, and the reduced mass corresponding to this motion is μ. l and j are the angular momenta associated with R and r, respectively. In all of our work on $NeBr_2$ we assume that the total angular momentum $J=0$, so that only even values of the Br_2 rotational quantum number (j) contribute to the calculation.

The X electronic state initial bound wave function is expanded as

$$\Psi_i(r,R,\theta)=\sum_{n_s'',n_b''} a^i_{n_s'',n_b''}\chi^i_0(r)\chi^i_{n_s''}(R)\chi^i_{n_b''}(\theta), \tag{2}$$

where $\chi^i_0(r)$ is the Br_2 $v=0$ wave function obtained by numerical integration of the X electronic state Rydberg–Klein–Rees (RKR) potential energy curve,[32] $\chi^i_{n_s''}(R)$ is a harmonic oscillator basis function used to describe the Ne–Br_2 stretch, and $\chi^i_{n_b''}(\theta)$ is a van der Waals bending basis function. These bending functions are obtained by expansion as a linear combination of spherical harmonic functions, with the expansion coefficients determined by diagonialization of the angular part of the vibrationally averaged Hamiltonian. For our calculations on $NeBr_2$, the initial bound wave function is composed of 15 harmonic oscillator functions with $R_e=3.67$ Å and $\omega=26.0$ cm^{-1}; our bending basis functions are a linear combination of 20 spherical harmonics (restricted to even values of j due to the symmetry of the Ne–Br_2 interaction potential).

The final (B electronic state) continuum wave function at energy E that yields Br_2 fragments in vibrational state v and rotational state j of the B electronic state is expanded as

$$\Psi_{fvjE}(r,R,\theta)=\sum_{v_c,j_c}\phi^{fvjE}_{v_c,j_c}(R)\chi^f_{v_c}(r)Y_{j_c,0}(\theta). \tag{3}$$

The $\chi^f_{v_c}(r)$ are the Br_2 bound vibrational wave functions, obtained by numerical integration of the Br_2 B electronic state RKR potential energy curve[32] and the $Y_{j_c,0}(\theta)$ are Br_2 free rotor wave functions. The resulting close-coupled equations are solved using the De Vogelaere integrator. The partial photodissociation cross section $\sigma_{fvjE\leftarrow i}$ is calculated by taking the squared overlap of the initial wave function Ψ_i with the continuum wave function Ψ_{fvjE}, thus determining the probability of producing, at energy E, a Br_2 fragment described by v, j in the B electronic state. (The electronic transition dipole is assumed constant over the energy range in question.) The total cross section,

$$\sigma_{fE\leftarrow i}=\sum_{v,j}\sigma_{fvjE\leftarrow i} \tag{4}$$

determines the photodissociation lineshape as a function of energy E. The distribution of fragment rotational and vibrational states is provided by,

$$P_{v,j}=\frac{\sigma_{fvjE\leftarrow i}}{\sigma_{fE\leftarrow i}}. \tag{5}$$

Finally, the total photofragmentation cross section is determined by integration of the line shape,

$$\sigma_{f\leftarrow i}=\int \sigma_{fE\leftarrow i}dE. \tag{6}$$

In a typical calculation of an excitation profile, we include a total of 5 Br_2 vibrational basis functions (v_c) and 20–30 rotational states (j_c) in each vibrational state. All of the j_c values are even in light of the symmetry of the intermolecular potential and the restriction to $J=0$. In general, the fragment quantum state distributions are more sensitive to the size of the basis set; we have checked the convergence of the fragment rotational and vibrational distributions by performing a limited number of calculations with a total of 6 vibrational functions. For low vibrational levels ($v\leqslant 22$) the fragment distributions are fully converged (within±5%). For higher vibrational levels, the rotational distributions are also fully converged, while the vibrational distributions are converged to within±10%.

When written in an expanded form, the expression for $\sigma_{fvjE\leftarrow i}$ is given by,

$$\sigma_{fvjE\leftarrow i}=|\langle\Psi_{fvjE}(r,R,\theta)|\Psi_i(r,R,\theta)\rangle|^2=\left|\sum_{n_s'',n_b''}\sum_{v_c,j_c}a^i_{n_s'',n_b''}\chi^i_{n_s''}(R)\chi^i_{n_b''}(\theta)\times\phi^{fvjE}_{v_c,j_c}(R)Y_{j_c,0}(\theta)F_{v_c,0}(r)\right|^2, \tag{7}$$

where

$$F_{v_c,0}(r)=\langle\chi^f_{v_c}(r)|\chi^i_0(r)\rangle \tag{8}$$

is the standard vibrational overlap integral between the $v=0$ level of the X electronic state in Br_2 and the $v=v_c$ vibrational level in the B state. As discussed below, we use the sensitivity of the cross section to the Br_2 vibrational overlap to deduce the contribution of various Br_2 basis functions to the overall excitation line shape.

The intermolecular potential used in this study is the same as that considered previously in classical trajectory studies of $NeBr_2$.[28] Briefly, the Ne–Br_2 interaction is written as the sum of two Ne–Br interactions, with the latter modeled as Morse potentials. The Morse parameters chosen ($D_e=42.0\,cm^{-1}$, $\alpha=1.67$ $Å^{-1}$, $R_{av}=3.90$ Å) were found in previous work to provide the correct equilibrium separation between the Ne atom and the center of mass of the Br_2, and

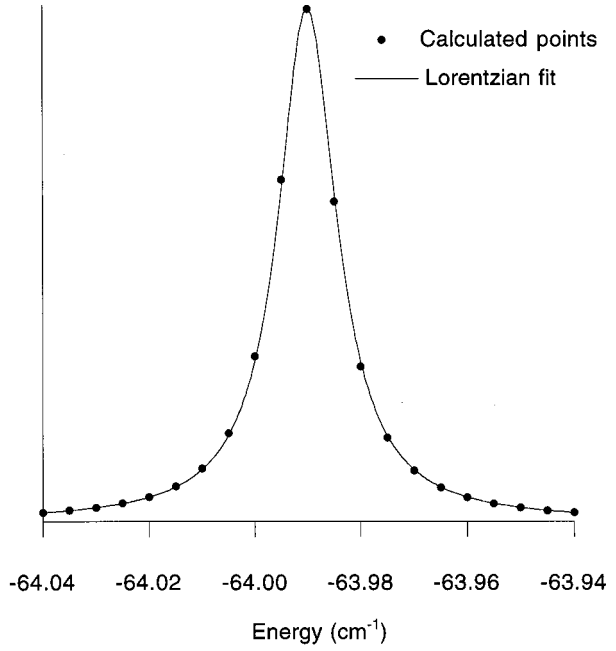

FIG. 2. Calculated excitation spectrum of $NeBr_2$, $v=10$, along with the best fit Lorentzian line shape. The energy axis (cm^{-1}) is relative to the $Ne+Br_2$ ($v=10$) energy asymptote.

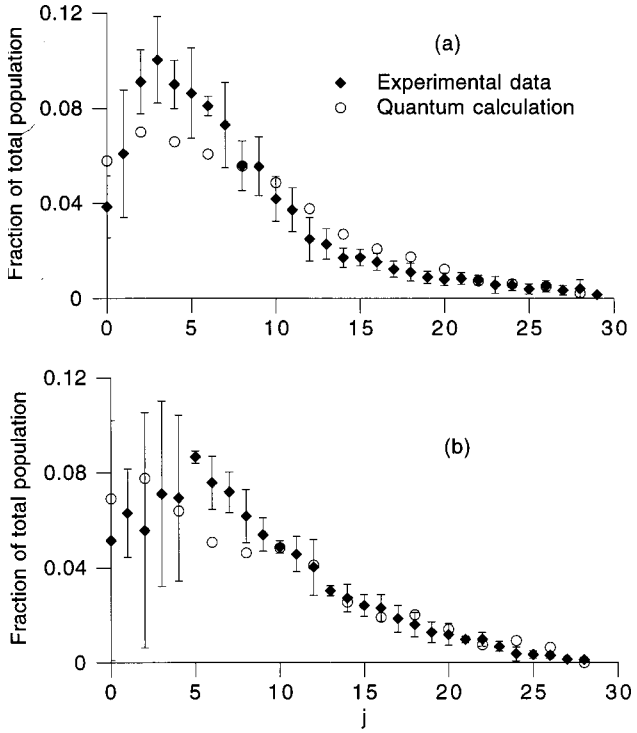

FIG. 3. Distribution of rotational states resulting from $\Delta v=-1$ dissociation of $NeBr_2$. (a) $v=9$ Br_2 fragments from $v=10$ $NeBr_2$; (b) $v=14$ Br_2 fragments from $v=15$ $NeBr_2$. The experimental data are from Ref. 28.

the correct dissociation energy for the $v=10$ $NeBr_2$ complex.[28] Since the goal of the present study is to make comparisons between the classical and quantum dynamics supported by this potential, no attempt has been made to refine the potential to improve, for example, the agreement between experimental and calculated fragment rotational distributions.

IV. RESULTS

In Fig. 2, we present the calculated photodissociation lineshape for $v=10$ $NeBr_2$, along with the best fit Lorentzian profile. (Except as noted below, all calculations have been carried out on the $Ne^{79}Br_2$ isotopic species.) The half-width of this line shape at half-maximum, 0.00674 cm^{-1}, allows one to calculate a photodissociation lifetime of 394 ps. These results are in excellent agreement with the high-resolution spectroscopic study of Thommen *et al.* in which the lifetime broadening of the spectrum was found to dictate a lifetime of 355 ps.[31] Further, the maximum in the line shape occurs at -63.99 cm^{-1} (relative to the energy of $v=10$ in uncomplexed Br_2), in excellent agreement with the experimentally determined D_0 of 64.3 ± 1.1 cm^{-1}.[28]

In Fig. 3(a), we display the calculated distribution of rotational populations for $v=9$ Br_2 fragments from the dissociation of $v=10$ $NeBr_2$, along with the experimental data.[28] Qualitatively, the agreement is excellent, with the calculated distribution extending to the energetic limit for this dissociation channel (as does the experimental data). While it is clear that the calculations overestimate slightly the role of the rotational states between 10 and 20 (and correspondingly underestimate the population in the lowest rotational states), the agreement with the overall shape and extent of the distribution is remarkable given the crude form of the intermolecular potential. In addition, the calculations are restricted to $J=0$ while the experimental distribution arises from excitation of an indeterminate number of total angular momentum states, with the exact number governed by the $NeBr_2$ rotational temperature in the free jet expansion, the degree of lifetime broadening, and the excitation laser bandwidth. In Fig. 3(b), the distribution of rotational populations calculated for $v=14$ fragments arising from the dissociation of $v=15$ $NeBr_2$ is shown, along with the experimental data. Again, the agreement with the experimental data is qualitatively correct, suggesting that the calculations are properly accounting for the variation of the rotational distributions with available energy. ($E_{avl}=67.7$ cm^{-1} for $v=9$ fragments and 48.7 cm^{-1} for $v=14$ fragments.[28])

Cline *et al.*, carried out high-resolution measurements of a number of $NeBr_2$ excitation features, and used these data to extract predissociation lifetimes.[30] In Table I, we present a comparison of our calculated lifetimes. These data are re-

TABLE I. Calculated and experimental lifetimes for $Ne^{79}Br_2$.

Vibrational level (v)	Experimental lifetime (ps)[a]	Calculated lifetime (ps)
10	355 ± 100	394
14	105 ± 10	126
15		102
16	95 ± 6	71
17	65 ± 6	61
19		35
20	35 ± 4	26

[a]Reference 30.

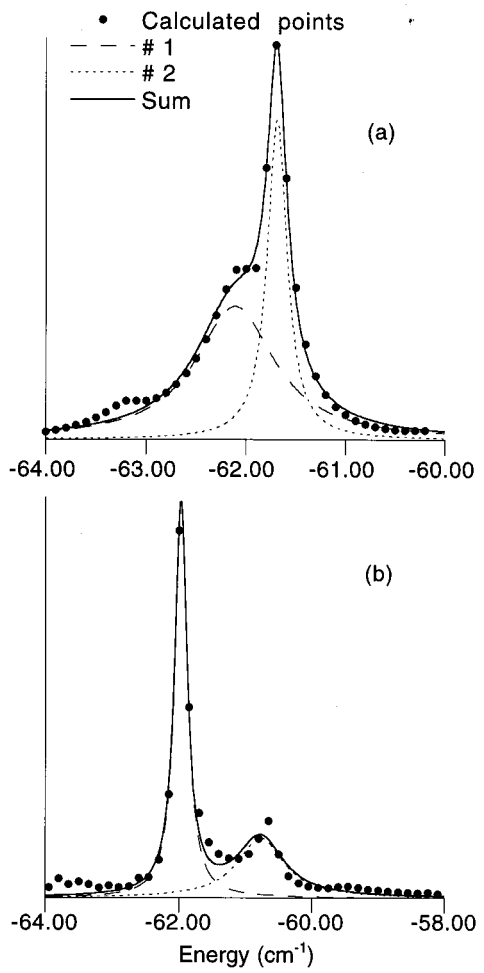

FIG. 4. Calculated excitation spectra of $NeBr_2$, along with the best fit sum-of-Lorentzians line shapes. The energy axes are relative to the $Ne+Br_2$ ($v=26$ or 27) energy asymptotes. (a) $v=26$ $NeBr_2$; (b) $v=27$ $NeBr_2$. The parameters for the Lorentzian fits in (a) are #1: HWHM=0.4822 cm^{-1}, centered at -62.11 cm^{-1}; #2: HWHM=0.1198 cm^{-1}, centered at -61.69 cm^{-1}. In (b), #1: HWHM=0.1098 cm^{-1}, centered at -61.97 cm^{-1}; #2: HWHM=0.5161 cm^{-1}, centered at -60.80 cm^{-1}.

stricted to particular vibrational states in the range of $v=10-20$ due to the limited availability of high resolution experimental data and the observation of single Lorentzian line shapes in the quantum calculations for vibrational levels $v<21$ only. As in the case of the rotational distributions, the agreement of the experimental and theoretical results is semiquantitative, with some of the calculated values lying within the experimental error bars, and others significantly outside the experimental uncertainties.

At higher vibrational levels, the quantum dynamics take on a different character. Beginning with $v=21$ ($E_{avl}=25.6\,cm^{-1}$), the line shapes are no longer well characterized by a single Lorentzian, and the fragment rotational distributions vary with excitation energy, even upon moving from low frequency side to the high frequency side of the same lineshape. These trends are continued for the highest vibrational levels for which dissociation in a $\Delta v=-1$ process is energetically possible. In Figs. 4(a) and 4(b), we display the excitation line shapes for the $v=26$ ($E_{avl}=5.4\,cm^{-1}$) and $v=27$ ($E_{avl}=2.3\,cm^{-1}$) $NeBr_2$ complexes.

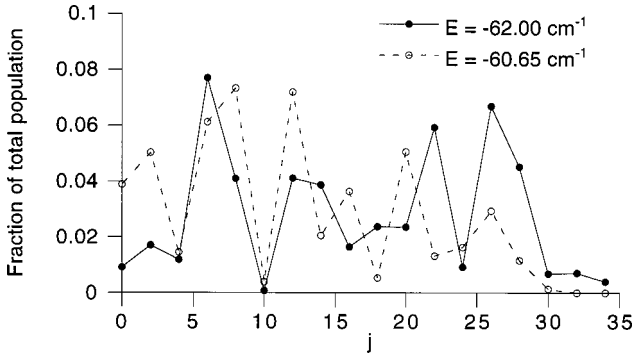

FIG. 5. Calculated rotational distributions for $v=25$ Br_2 fragments from the dissociation of $v=27$ $NeBr_2$ at the energies corresponding to the peaks in the excitation spectrum [see Fig. 4(b)].

For these vibrational levels, the non-Lorentzian character of the line shape is clear, and for $v=27$ two distinct resonances are present. The figures show, however, that the spectra are well represented by a sum of two Lorentzian line shapes. We have also examined the $v=25$ fragment rotational distributions arising at the energies of the two closely spaced resonances for $v=27$ $NeBr_2$. In Fig. 5, these distributions are compared, clearly demonstrating that the dynamics following excitation at these two energies differ in a significant way.

As shown in Fig. 6, we have also carried out calculations for the $Ne^{81}Br_2$ complex. The $v=27$ excitation line shape for this species also shows two distinct resonances, but the spacing and relative intensities are quite different from those observed for $Ne^{79}Br_2$. Clearly, the phenomenon that causes more than one single Lorentzian line shape is sensitive to the available energy ($E_{avl}=2.8\,cm^{-1}$ for $Ne^{81}Br_2$, as compared

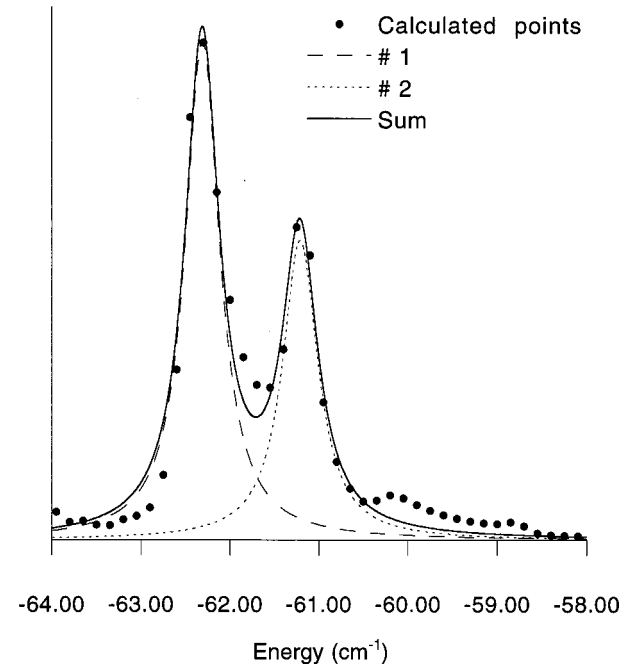

FIG. 6. Calculated excitation spectrum of $Ne^{81}Br_2$, along with best fit sum-of-Lorentzians line shapes. The energy axis (cm^{-1}) is relative to the $Ne+^{81}Br_2$ ($v=27$) energy asymptote. The parameters for the Lorentzian fits are, #1: HWHM=0.2344 cm^{-1}, centered at -62.31 cm^{-1}; #2: HWHM =0.2419 cm^{-1}, centered at -61.21 cm^{-1}.

TABLE II. Calculated and experimental vibrational branching ratios for $Ne^{79}Br_2$ in the B electronic state.

Vibrational level (v)	Calculated distribution				Experimental distribution[a]			
	$\Delta v=-1$	$\Delta v=-2$	$\Delta v=-3$	$\Delta v=-4$	$\Delta v=-1$	$\Delta v=-2$	$\Delta v=-3$	$\Delta v=-4$
10	0.98	0.02	⋯	⋯	1	⋯	⋯	⋯
14	0.96	0.04	⋯	⋯				
15	0.95	0.05	⋯	⋯				
16	0.94	0.06	⋯	⋯				
17	0.93	0.06	0.01	⋯				
19	0.91	0.08	0.01	⋯				
20	0.87	0.12	0.01	⋯				
21	0.87	0.12	0.01	⋯				
22	0.82	0.15	0.03	⋯	0.7	0.1	0.07	0.07
24	0.71	0.23	0.06	⋯				
25	0.59	0.30	0.09	0.01				
26	0.59	0.31	0.08	0.01				
27[b]	0.16	0.66	0.15	0.03	0.3	0.4	0.2	0.1
27[c]	0.08	0.62	0.24	0.05				

[a]Reference 30.
[b]Lower energy peak.
[c]Higher energy peak.

with 2.3 cm^{-1} for $Ne^{79}Br_2$ assuming the same dissociation energy for the two isotopes) or the underlying rotational level spacing, or both.

In Table II, we present the calculated fragment vibrational state distributions for $Ne^{79}Br_2$, along with the limited experimental data.[30] The vibrational distributions are consistent with the general ''energy gap'' result that $\Delta v=-1$ fragmentation pathways are favored for all vibrational levels, except for those very near the energetic threshold for that dissociation channel. For $v=27$, we find that the probability of producing $v=26$ Br_2 fragments are distinctly different for the two separate peaks that we have identified in the excitation profile.

V. DISCUSSION

A. Dynamics at high values of E_{avl}

As shown in Fig. 2, for high values of E_{avl}, the quantum calculations predict excitation features that are well represented by single Lorentzian line shapes. Further, the dependence of the linewidth on vibrational level is qualitatively in accord with the experimental data (Table I). For these vibrational states, the agreement of the calculated and experimental Br_2 fragment rotational distributions is nearly quantitative. We conclude from these examples that the model intermolecular potential is adequate to reproduce the gross trends in the experimental data. Clearly, however, refinement of the potential energy surface and/or thermal averaging over the manifold of rotational states prepared in the experimental investigations will be required to achieve quantitative agreement.

It is significant to note that the quantum calculations correctly reproduce the breadth of the Br_2 fragment rotational distributions. The premature truncation of the calculated fragment distributions was a fundamental failing of the classical trajectory model, as applied to $NeBr_2$.[28] The origin, therefore, of this disparity lies in the assumptions inherent in the classical model and not in the failure of the potential energy surface to incorporate an adequate degree of angular anisotropy. This result reinforces the conclusion of Nejad-Sattari and Stephenson, who noted that the classical model must fail whenever the kinematics of angular momentum transfer do not dominate the dynamics.[28] For many of the rare gas/halogen complexes, it is clear that energetic considerations are more important in determining the extent of rotational excitation. Clearly, the mechanisms by which the halogen fragment achieves a high level of rotational excitation are more subtle than provided in the classical model. Of particular note are (1) the absence, in the classical model calculations, of consideration of the mechanism of the intramolecular vibrational redistribution that must accompany the dissociation and (2) the restriction to a total angular momentum of zero. (Note, however, that the latter restriction also applies to the quantum calculations reported in this manuscript.)

B. Dynamics at low values of E_{avl}

The results displayed in Figs. 4–6 for low values of E_{avl} are highly reminiscent of those presented by Halberstadt *et al.* in their examination of intramolecular vibrational redistribution (IVR) in $ArCl_2$.[4] For this species, multiple Lorentzian line shapes are observed in the quantum calculations when the dissociation channel corresponding to the loss of only one halogen quantum vibration is energetically closed. The calculations of Halberstadt *et al.* clearly demonstrate that the origin of the multiple resonances is IVR in the small molecule limit—the optically active, quasibound level correlating with vibrational level v is coupled to a sparse manifold of ''dark'' states (also quasibound) that correlate with $v-1$. These ''dark'' states are then coupled to the $v-2$ dissociative continuum. The relative intensities of the multiple peaks are determined by the strength of the interaction between the optically active (''bright'') state and the ''dark'' states, and well as the degree of resonance between the ''bright'' and ''dark'' states. One signature characteristic of this phenomenon is $\Delta v=-2$ rotational distributions that

vary widely with slight changes in energy, as the variable identity of the intermediate ''dark'' state strongly influences the dissociation dynamics.[4]

The significant difference between our present results and the $ArCl_2$ study summarized above is that for $NeBr_2$, *we observe multiple resonances and widely varying* $\Delta v=-2$ *fragment rotational distributions when the* $\Delta v=-1$ *dissociation channel remains energetically open*, albeit with very limited amounts of energy available for fragment translational and rotational excitation. Thus, if judged by energy alone, there are no quasibound, intermediate ''dark'' states available to interact with the optically active level. The current calculations (and the classical results) suggest, however, that imbedded in the nominal dissociative continuum are states that have significant lifetimes, corresponding to fragments localized in the region of the attractive well in the intermolecular potential. To explore further the physical basis of these results, we have carried out two additional sets of calculations, as described below.

1. Limited basis set calculations

In a typical calculation of the $v=27$ resonance region [Fig. 4(b)], the basis set consists of 5 Br_2 vibrational wave functions, $v=24-28$. If it is true that some continuum states are partially localized in the intermolecular region, then these states may have sufficient overlap with the ground electronic state $NeBr_2$ wave function to generate an excitation spectrum. To test this hypothesis, we performed calculations in which the basis set was restricted to exclude the zeroth-order quasibound level. Specifically, we included only $v=24$, 25, and 26 in a calculation of the $v=27$ resonance, with the goal of determining whether the continuum states are localized in the attractive region of the intermolecular potential. The results of this calculation are shown in Fig. 7, along the spectrum obtained in the full basis set calculation. The continuum only calculation shows clearly defined structure at the same energy as the smaller of the two resonances in the full calculation. We conclude from this result that the higher energy resonance in the full calculation results from an interaction between the quasibound optically active state and a long-lived resonance imbedded in the nominal dissociative continuum. The continuum resonance appears at significantly higher intensity in the spectrum resulting from the full basis set calculation by borrowing intensity from the more dominant optically active quasibound state.

Confirmation of this result can be found when we consider the $v=27$ resonance in the $Ne^{81}Br_2$ molecule. A comparison of Figs. 4(b) and 6 demonstrates that the position and relative intensities of the resonances vary with isotopic substitution. When we carry out the reduced basis set calculation on $Ne^{81}Br_2$, we find a pattern of optical activity in the continuum that is identical to that observed in $Ne^{79}Br_2$. For $Ne^{81}Br_2$, however, the continuum resonance is shifted to lie at the same energy as the higher energy resonance in the full calculation.

As noted previously, the rotational distributions calculated for the $v=25$ fragments that arise from dissociation of $v=27$ $NeBr_2$ are significantly different following excitation of the two resonances observed (Fig. 5). We interpret this result as arising from two different mechanisms for the dissociation. At the energy corresponding to the peak of the higher energy resonance, dissociation proceeds via coupling to an intermediate resonance in the continuum. This mechanism is common to both the $Ne^{79}Br_2$ and $Ne^{81}Br_2$ species. In Fig. 8(a), we display three different rotational distributions.

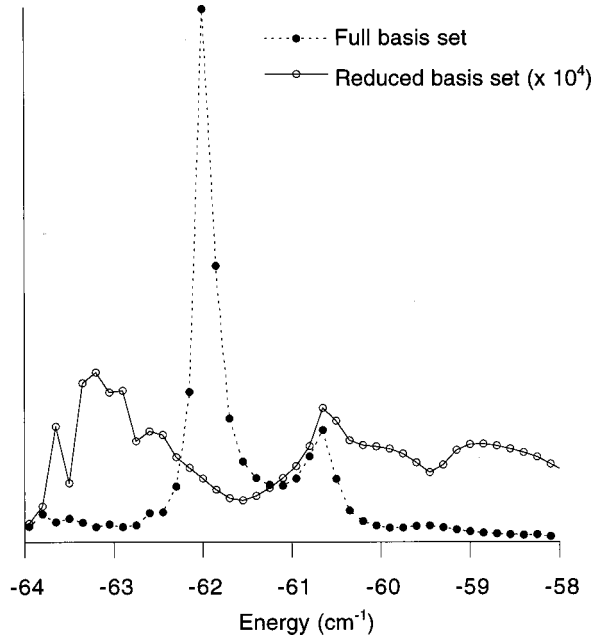

FIG. 7. Calculated excitation spectra of $NeBr_2$, both quasibound (closed circles) and continuum (open circles). The closed circles are the same points as in Fig. 4(b). The solid and dashed lines are intended to guide the eye and do not represent fits to the points.

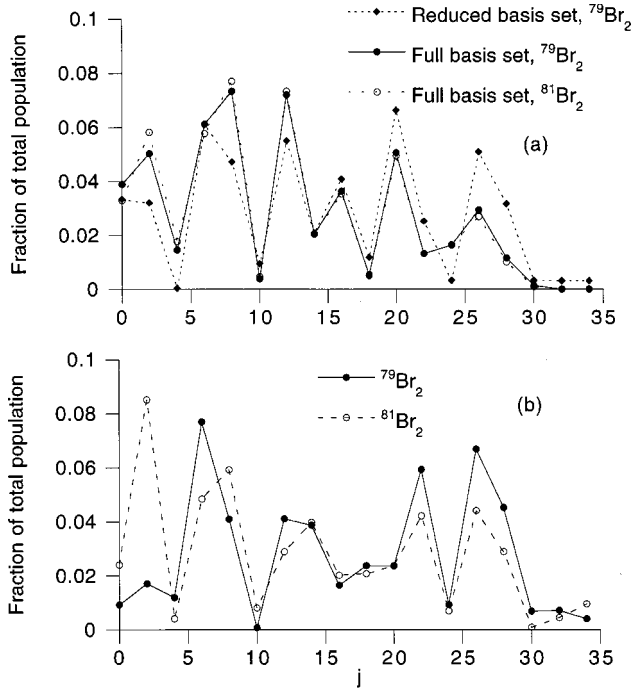

FIG. 8. Isotopic, basis set, and energy dependence of the $v=25$ Br_2 fragment rotational distribution that results from the dissociation of $NeBr_2$, $v=27$. (a) Excitation at the higher energy feature in the excitation spectra; (b) excitation of the lower energy feature in the excitation spectra.

Two of these distributions are simply those derived from full calculations on the two different isotopic species, and are nearly identical. The third distribution is obtained from the reduced basis set calculation at the energy of the higher energy peak for the $Ne^{79}Br_2$ species. Clearly, all of these distributions are very similar, and this observation is evidence that excitation of $NeBr_2$ at the peak of the higher energy feature dissociates via the resonance identified in the reduced basis set calculation.

It is tempting to assign the lower energy resonance to dissociation via direct coupling to the dissociative continua ($\Delta v=-1$ and $\Delta v=-2$). This assignment, however, is difficult to substantiate. We would expect the rotational distributions arising from direct coupling to be relatively smooth. For comparison, the available energy of the $\Delta v=-2$ dissociation of $v=27$ $NeBr_2$, 69.6 cm^{-1}, is nearly the same as that for the $\Delta v=-1$ dissociation of $v=10$, 67.7 cm^{-1}.[28] Ignoring the relatively minor impact of changing rotational constants, we expect direct dissociation events with similar E_{avl}'s to result in qualitatively similar rotational distributions. Inspection of Figs. 3(a) and 5 demonstrates that this is not the case. In addition, we expect little isotope dependence of the rotational distributions. The distributions for the $^{79}Br_2$ and $^{81}Br_2$ fragments in Fig. 8(b) are quite similar, but the deviations shown at small j are larger than we expect for the direct dissociation of such comparable species. Finally, direct dissociation of species with comparable reduced mass and available energy should occur with comparable lifetime. A comparison of Figs. 4(b) and 6 shows, however, that the linewidth of the lower energy resonance in $Ne^{81}Br_2$ is wider than that for $Ne^{79}Br_2$ by approximately a factor of 2. The mechanism by which such widely varying lifetimes and erratic rotational distributions appear for the lower energy resonance remains unclear, but one possibility is quantum interference between two paths leading to $v=25$ fragments; (1) direct dissociation to the $\Delta v=-2$ continuum; (2) indirect, stepwise dissociation via two $\Delta v=-1$ processes. In this light, it is significant to note that, for excitation at the lower energy peak, the vibrational branching ratios are very different for the isotopic species, with 15.9% of all fragments appearing in $v=26$ ($\Delta v=-1$) for $Ne^{79}Br_2$, while 27.0% of the $^{81}Br_2$ fragments are in $v=26$. The relevant branching percentages for $v=25$ fragments are 65.9% ($^{79}Br_2$) and 52.3% ($^{81}Br_2$).

2. Calculations with selective vibrational overlaps

We have noted, in Eqs. (7) and (8), the importance of the $B\leftarrow X$ Br_2 vibrational overlap integrals in modulating the overall excitation cross section. Thus, we have an opportunity to explore the contributions of the various vibrational basis functions to the quasibound $NeBr_2$ wave function. Since the $NeBr_2$ ground electronic state, $v=0$ bound state wave function is localized in the region of the attractive well in the intermolecular potential, the photofragmentation cross section is greater than zero only when the quasibound, B electronic state wave function has non-zero amplitude in that same region. In a zeroth order picture, only one vibrational basis function contributes to the $NeBr_2$ wave function. If, for example, we consider the $v=10$ vibrational level of $NeBr_2$ in the B state, a first approximation is to consider that only the $v=10$ Br_2 vibrational basis function contributes to the quasibound wave function. The results of the full calculation of this excitation profile are shown in Fig. 2. We have also performed a second calculation on $v=10$ $NeBr_2$, however, in which the full basis is used, but the vibrational overlap integral for the Br_2 (10,0) $B\leftarrow X$ transition is set to 0. Thus, we can deduce the relative contributions of the $v=10$ and $v\neq 10$ vibrational basis functions to the $NeBr_2$ wave function in the region of the attractive well in the intermolecular potential. For $v=10$, we find that setting the (10,0) overlap integral to 0 results in a decrease in the integrated photofragmentation cross section by a factor of 3.8×10^5, though the overall appearance and linewidth of the excitation feature is unchanged. As expected, the basis functions with $v\neq 10$ make only a small contribution to the photofragmentation cross section. This result suggests that when E_{avl} is high, the oscillator strength in the excitation is carried nearly exclusively by the zeroth order quasibound wave function.

This situation becomes significantly more complicated as v increases (E_{avl} decreases). Specifically, for vibrational level $v=v_0$ in $NeBr_2$, the contribution of the $v\neq v_0$ basis functions increases sharply with increasing v_0. For $v_0=27$, the decrease in the integrated photofragmentation cross section [when the (27,0) Br_2 $B\leftarrow X$ vibrational overlap integral is set to 0] is only 2100, when both the higher and lower energy peaks are considered. In addition, the impact of setting the $v=27$ vibrational overlap to zero is more significant for the lower energy feature than the higher energy feature. This result is consistent with our premise that the higher energy peak represents excitation of ''continuum'' states with significant amplitude in the optically accessible region of the intermolecular potential energy surface.

Finally, the behavior that we have identified in $NeBr_2$ is quite similar to that explored by González-Lezana *et al.* in their quantum calculations on $HeBr_2$ (Ref. 22) and Janda *et al.* on $ArCl_2$.[24] Specifically, in $HeBr_2$, excitation just below the energetic closing of the $\Delta v=-1$ dissociation channel ($v=43$), results in excitation features that contain multiple peaks. In addition, the fragment rotational distributions are quite structured, and vary for the two principle peaks in the excitation spectrum, just as we observe for $NeBr_2$ (Fig. 5). In $ArCl_2$, Janda *et al.* examined the dependence of the calculated vibrational predissociation lifetime on small variations in the potential parameters at energies when the $\Delta v=-1$ dissociation channel is open, but with low values of E_{avl}. The striking result is that some values of the potential parameters result in lifetimes that are extraordinarily long. These workers show that the anomalous lifetimes arise from a degeneracy of the initially excited state with a long-lived resonance in the $\Delta v=-1$ continuum. Further calculations suggest that the resonance originates from rotationally predissociative states in the $\Delta v=-1$ manifold—states that are trapped by an effective centrifugal barrier to dissociation.[24] The previously described classical calculations on the dissociation of $NeBr_2$ support the rotational predissociation mechanism,[28] but generalize it to include states that achieve a high degree of fragment rotational excitation, albeit temporarily. These states are not necessarily confined by a centrifu-

gal barrier, but have long lifetimes because they contain energy that is momentarily stored in rotational channels that are asymptotically closed. The current quantum calculations on $NeBr_2$ do not allow us to further illuminate the mechanism that gives rise to the continuum resonances. Our results demonstrate, however, that the presence of long-lived resonances at low energies in the dissociative continuum may be a general phenomenon for rare gas/halogen van der Waals complexes.

VI. CONCLUSIONS

These calculations provide a semiquantitative test of the simplified potential energy surface used in previous investigations of the dissociation of $NeBr_2$.[28] While the agreement with the experimental data is not perfect, the accuracy is sufficient to conclude that the failings identified in previous classical trajectory studies are fundamental to that approach, and do not reflect any gross inadequacy of the potential energy surface. It is not possible to conclude a definitive link between the orbiting resonances observed in the classical trajectory calculations, and the quantum dynamics discussed in this paper. We believe that the data strongly suggest that the features in the classical dynamics do have a quantum mechanical analog. A more conclusive link could be established by direct examination of the quantum mechanical wave functions at low energies of E_{avl}. Wave packet studies may provide this link, and would be of considerable assistance in deducing the value of the classical calculations in identifying dynamical properties of experimental importance.

ACKNOWLEDGMENTS

The research has been supported by a grant from the National Science Foundation (CHE-9223565). T.A.S. is grateful for the support of the Camille and Henry Dreyfus Foundation in the form of a Henry Dreyfus Teacher–Scholar Award (1994–1999). These calculations were initiated while T.A.S. was on sabbatical leave at the University of Pennsylvania in 1997; the hospitality of Professor Marsha Lester and her grant of significant computer time are gratefully acknowledged.

[1] See, for example, W. H. Miller, Annu. Rev. Phys. Chem. **41**, 245 (1990); G. C. Schatz, *ibid.* **39**, 317 (1988).
[2] J. A. Beswick and J. Jortner, Adv. Chem. Phys. **47**, 363 (1981).
[3] O. Roncero, J. A. Beswick, N. Halberstadt, P. Villarreal, and G. Delgado-Barrio, J. Chem. Phys. **92**, 3348 (1990).
[4] N. Halberstadt, S. Serna, O. Roncero, and K. C. Janda, J. Chem. Phys. **97**, 341 (1992).
[5] N. Halberstadt, J. A. Beswick, and K. C. Janda, J. Chem. Phys. **87**, 3966 (1987).
[6] R. L. Waterland, M. I. Lester, and N. Halberstadt, J. Chem. Phys. **92**, 4261 (1990).
[7] S. K. Gray and C. E. Wozny, J. Chem. Phys. **94**, 2817 (1991).
[8] N. Halberstadt, J. A. Beswick, O. Roncero, and K. C. Janda, J. Chem. Phys. **96**, 2404 (1992).
[9] N. Halberstadt, O. Roncero, and J. A. Beswick, Chem. Phys. **129**, 83 (1989).
[10] J. A. Beswick and G. Delgado-Barrio, J. Chem. Phys. **73**, 3653 (1980).
[11] O. Roncero, J. A. Beswick, N. Halberstadt, P. Villarreal, and G. Delgado-Barrio, J. Chem. Phys. **92**, 3348 (1990).
[12] G. E. Ewing, J. Phys. Chem. **91**, 4662 (1987).
[13] A. A. Buchachenko, A. Y. Balsogolov, and N. F. Stepanov, J. Chem. Soc., Faraday Trans. **90**, 3229 (1994).
[14] S. S. Huang, C. R. Bieler, K. C. Janda, F-M Tao, W. Klemperer, P. Casavecchia, G. G. Volpi, and N. Halberstadt, J. Chem. Phys. **102**, 8846 (1995).
[15] O. Roncero, P. Villarreal, G. Delgado-Barrio, N. Halberstadt, and K. C. Janda, J. Chem. Phys. **99**, 1035 (1993).
[16] O. Roncero and S. K. Gray, J. Chem. Phys. **104**, 4999 (1996); S. K. Gray and O. Roncero, J. Phys. Chem. **99**, 2512 (1995).
[17] O. Roncero, N. Halberstadt, and J. A. Beswick, J. Chem. Phys. **104**, 7554 (1996).
[18] A. A. Buchachenko, T. Gonzalez-Lezana, M. I. Hernandez, G. Delgado-Barrio, P. Villarreal, and N. F. Stepanov, Chem. Phys. Lett. **269**, 448 (1997).
[19] D. G. Jahn, W. S. Barney, J. Cabalo, S. G. Clement, A. Rohrbacher, T. J. Slotterback, J. Williams, and K. C. Janda, J. Chem. Phys. **104**, 3501 (1996).
[20] T. González-Lezana, Marta I. Hernández, G. Delgado-Barrio, and P. Villarreal, J. Chem. Phys. **106**, 3216 (1997).
[21] A. Rohrbacher, T. Ruchti, K. C. Janda, A. A. Buchachenko, M. I. Hernández, T. González-Lezana, P. Villarreal, and G. Delgado-Barrio, J. Chem. Phys. **110**, 256 (1999).
[22] T. González-Lezana, Marta I. Hernández, G. Delgado-Barrio, A. A. Buchachenko, and P. Villarreal, J. Chem. Phys. **105**, 7454 (1996).
[23] S. Zamith, C. Meier, N. Halberstadt, and J. A. Beswick, J. Chem. Phys. **110**, 960 (1999).
[24] K. C. Janda, O. Roncero, and N. Halberstadt, J. Chem. Phys. **105**, 5830 (1996).
[25] A. A. Buchachenko and N. F. Stepanov, Spectrosc. Lett. **25**, 189 (1992).
[26] R. L. Waterland, J. M. Skene, and M. I. Lester, J. Chem. Phys. **89**, 7277 (1988).
[27] T. A. Stephenson, J. Chem. Phys. **97**, 6262 (1992).
[28] M. Nejad-Sattari and T. A. Stephenson, J. Chem. Phys. **106**, 5454 (1997).
[29] B. A. Swartz, D. E. Brinza, C. M. Western, and K. C. Janda, J. Phys. Chem. **88**, 6272 (1984).
[30] J. I. Cline, D. D. Evard, B. P. Reid, N. Sivakumar, F. Thommen, and K. C. Janda, in *Structure and Dynamics of Weakly Bound Molecular Complexes*, edited by Alfons Weber (Reidel, Dordrecht, 1987), pp. 533–551.
[31] F. Thommen, D. D. Evard, and K. C. Janda, J. Chem. Phys. **82**, 5295 (1985).
[32] R. F. Barrow, T. C. Clark, J. A. Coxon, and K. K. Yee, J. Mol. Spectrosc. **51**, 428 (1974).